

Geophysical Research Letters®



RESEARCH LETTER

10.1029/2021GL097568

Insights Into the Aerodynamic Versus Radiometric Surface Temperature Debate in Thermal-Based Evaporation Modeling

Key Points:

- Aerodynamic temperature and evaporation well estimated from physical principles and available energy-water limits in different ecosystems
- Water stress and vegetation cover influences the difference between aerodynamic and radiometric temperatures through plant homeostasis
- Non-parametric model offers a parameter-sparse approach describing evaporation, canopy conductance and vapor pressure deficit relationship

Supporting Information:

Supporting Information may be found in the online version of this article.

Correspondence to:

K. Mallick,
kaniska.mallick@gmail.com;
kaniska.mallick@list.lu

Citation:











Mallick, K., Baldocchi, D., Jarvis, A., Hu, T., Trebs, I., Sulis, M., et al. (2022). Insights into the aerodynamic versus radiometric surface temperature debate in thermal-based evaporation modeling. *Geophysical Research Letters*, 49, e2021GL097568. <https://doi.org/10.1029/2021GL097568>

Received 4 JAN 2022

Accepted 6 JUL 2022

Author Contributions:

Conceptualization: Kaniska Mallick, Dennis Baldocchi
Data curation: Christian Bossung, Yomna Eid, Nina Hinko-Najera, Wayne S. Meyer
Formal analysis: Kaniska Mallick
Funding acquisition: Kaniska Mallick
Investigation: Kaniska Mallick
Methodology: Kaniska Mallick

Kaniska Mallick^{1,2} , **Dennis Baldocchi**² , **Andrew Jarvis**³, **Tian Hu**¹, **Ivonne Trebs**¹, **Mauro Sulis**¹ , **Nishan Bhattarai**⁴, **Christian Bossung**¹, **Yomna Eid**⁵ , **Jamie Cleverly**⁶ , **Jason Beringer**⁷ , **William Woodgate**^{8,9}, **Richard Silberstein**^{7,10} , **Nina Hinko-Najera**¹¹, **Wayne S. Meyer**¹² , **Darren Ghent**¹³, **Zoltan Szantoi**^{14,15} , **Gilles Boulet**¹⁶, and **William P. Kustas**⁴ 

¹Department of Environmental Research and Innovation, Luxembourg Institute of Science and Technology, Belvaux, Luxembourg, ²Department of Environmental Science Policy and Management, University of California, Berkeley, CA, USA, ³Lancaster Environment Centre, Lancaster University, Lancaster, UK, ⁴Hydrology and Remote Sensing Laboratory, USDA-ARS, Beltsville, MD, USA, ⁵The Julius Maximilians University of Würzburg, Würzburg, Germany, ⁶Terrestrial Ecosystem Research Network, College of Science and Engineering, James Cook University, Cairns, QLD, Australia, ⁷School of Agriculture and Environment, The University of Western Australia, Perth, WA, Australia, ⁸School of Earth and Environment, The University of Western Australia, Perth, WA, Australia, ⁹School of Earth and Environmental Sciences, The University of Queensland, Brisbane, QLD, Australia, ¹⁰School of Science, Edith Cowan University, Joondalup, WA, Australia, ¹¹School of Ecosystem and Forest Sciences, The University of Melbourne, Creswick, VIC, Australia, ¹²School of Biological Sciences, University of Adelaide, Adelaide, SA, Australia, ¹³Department of Physics and Astronomy, University of Leicester, Leicester, UK, ¹⁴Science, Applications & Climate Department, European Space Agency, Frascati, Italy, ¹⁵Department of Geography & Environmental Studies, Stellenbosch University, Stellenbosch, South Africa, ¹⁶Centre d'Etudes Spatiales de la Biosphère, Toulouse, France

Abstract Global evaporation monitoring from Earth observation thermal infrared satellite missions is historically challenged due to the unavailability of any direct measurements of aerodynamic temperature. State-of-the-art one-source evaporation models use remotely sensed radiometric surface temperature as a substitute for the aerodynamic temperature and apply empirical corrections to accommodate for their inequality. This introduces substantial uncertainty in operational drought mapping over complex landscapes. By employing a non-parametric model, we show that evaporation can be directly retrieved from thermal satellite data without the need of any empirical correction. Independent evaluation of evaporation in a broad spectrum of biome and aridity yielded statistically significant results when compared with eddy covariance observations. While our simplified model provides a new perspective to advance spatio-temporal evaporation mapping from any thermal remote sensing mission, the direct retrieval of aerodynamic temperature also generates the highly required insight on the critical role of biophysical interactions in global evaporation research.

Plain Language Summary Water lost by plants through evaporation is strongly linked with the temperature at an unknown height within the canopy. Because this in-canopy temperature cannot be typically measured by a satellite, the majority of the global evaporation models substitute this with skin temperature, or the near-surface temperature observed by the satellite sensors. Such methods do not fully capture the physical and biological processes governing the magnitude and variability of plant water use under severe water stress, leading to substantial errors in water cycle monitoring in the dry regions. Here, we show how a simple model that requires no anticipated parameter, provides not only reasonable estimates of evaporation in a variety of dry and wet conditions, but also a better insight into the role of plant water stress and greenness in the difference between the in-canopy temperature and skin temperature. This model offers an alternative and novel perspective that can be used in images from current and future thermal satellite missions to advance global plant water use mapping for several water management applications and to investigate the highly complex land-atmosphere interactions and feedback mechanisms.

© 2022 The Authors.

This is an open access article under the terms of the [Creative Commons Attribution-NonCommercial License](https://creativecommons.org/licenses/by/4.0/), which permits use, distribution and reproduction in any medium, provided the original work is properly cited and is not used for commercial purposes.

1. Introduction

With the acceleration in climate warming and land surface drying, the role of temperature on water cycle becomes increasingly critical due to its effect on the evaporation component. Theoretically, evaporation (E) from vegetated canopies depends on the temperature at the canopy-air space, which is also called the aerodynamic temperature (T_0). Because T_0 is not measurable at the global scale, operational E mapping from thermal infrared (TIR) Earth

Project Administration: Kaniska Mallick

Resources: Kaniska Mallick, Jason Beringer, Darren Ghent

Validation: Kaniska Mallick

Writing – original draft: Kaniska Mallick

Writing – review & editing: Dennis Baldocchi, Andrew Jarvis, Tian Hu, Ivonne Trebs, Mauro Sulis, Nishan Bhattarai, Jamie Cleverly, William Woodgate, Richard Silberstein, Darren Ghent, Zoltan Szantoi, Gilles Boulet, William P. Kustas

observation satellite missions routinely use the radiometric surface temperature (T_r) measured by the satellite sensors as a proxy for T_0 (Boulet et al., 2012). However, these two temperatures are not equal. While T_r corresponds to a weighted soil and vegetation temperature, T_0 represents an extrapolated air temperature within the vegetation canopy at which the vertical flow of water vapor occurs during evaporation (Kustas et al., 2007). T_r and T_0 differs by several degrees (Chehbouni et al., 1996, 2001) and using them interchangeably in operational E models may lead to large errors in vegetation water use computation and water cycle monitoring, particularly over complex landscapes of arid and semiarid climates (Verhoef et al., 1997). To accommodate the inequality between these two temperatures, common global evaporation models use empirical fitting parameters (Boulet et al., 2012; Garratt & Hicks, 1973; Lhomme et al., 1997; Verma, 1989) or contrasting parameterizations of unobserved variables (Li et al., 2019; Troufleau et al., 1997; Young et al., 2021), which introduce additional uncertainties in the models.

For advancing water cycle monitoring and irrigation management in the dry regions from current and future TIR satellite missions, it is crucial to retrieve global evaporation using fundamental theoretical principles and reduce our reliance on empirical parameters in the operational evaporation models. A major challenge, however, is the non-linear dependency of evaporation not only on T_0 but also on additional biophysical attributes of vegetation which cannot be measured directly at the global scales, such as the aerodynamic conductance and canopy-surface conductance, respectively. Therefore, a viable approach to address this challenge is to estimate evaporation by directly constraining T_0 and conductances through T_r in a non-parametric modeling framework.

Such a non-parametric formulation, called Surface Temperature Initiated Closure (STIC) has been shown to provide reasonable estimates of evaporative fluxes across contrasting biomes and aridity in the northern and southern hemispheres (Bai et al., 2021; Bhattarai et al., 2018, 2019; Mallick et al., 2014, 2016, 2018; Trebs et al., 2021). However, it is equally important to explain the long-debated T_r versus T_0 differences from the theoretical standpoint to simplify the operational evaporation retrievals from current and future TIR satellite missions. This will provide sound method to derive the impacts of climate warming on global evaporation variability and ecosystem water use strategies.

Here, we employ STIC to gain insights into the physical connection between T_0 and T_r , and understanding the role of environmental as well as biophysical factors in controlling their differences. For predicting T_0 and E , we used remote sensing based T_r in conjunction with environmental observations as the main forcings at 10 eddy covariance (EC) sites from different ecological transects and aridity classes in Australia (eight) and the United States (two). We evaluated the retrieved T_0 by comparing with reference T_0 values, which were obtained by inverting the Surface Energy Balance (SEB) flux observations. We subsequently analyzed T_0 versus T_r relationship and assessed the role of available energy and water stress on their differences. We further investigated the extent to which the interactions between SEB components and biophysical conductances control the differences between these two temperatures under different soil and atmospheric water stress. We finally evaluated the accuracy of E and sensible heat flux (H) retrievals.

Section 2 provides a brief description of STIC, remote sensing data, and the observations used at the 10 sites. Section 3 describes the results and associated discussions. In Section 4, we conclude with an outlook on a potential step forward for rethinking and simplifying thermal evaporation models and the utility of STIC to study the spatio-temporal variability of evaporation and land-atmosphere interactions.

2. Methods and Data

2.1. Model Based Retrieval of T_0

To constrain evaporation using a non-parametric approach, we perceive the vegetation-atmosphere system as a box and consider evaporation as both the driver and driven by the biophysical states in the vegetation-atmosphere system (Figure S1a in Supporting Information S1). Assuming the surface-atmosphere exchange inside the box is operated within the available environmental and water limits, we can estimate evaporation by finding analytical solution of the biophysical states from the known boundary conditions of the box that is, solar radiation (R_G), air temperature (T_a), humidity (rH), and T_r . This yields a non-parametric formulation of evaporation in the framework of SEB and the model is named as STIC (Figure S1b in Supporting Information S1) (Bhattarai et al., 2018; Mallick et al., 2018; Trebs et al., 2021).

Surface Temperature Initiated Closure is a single-source SEB model and the explicit assumptions of STIC include the (a) first order dependence of evaporative fraction (F_E) on an aggregated water stress index (I_{SM}), aerodynamic and canopy-surface conductance; (b) first order dependence of T_0 on F_E and I_{SM} ; (c) first order dependence of aerodynamic conductance (g_a) on T_0 and net available energy; (d) the dependence of canopy-surface conductance (g_{cs}) on T_0 , net available energy, g_a , and vapor pressures of air and source/sink height; and (e) direct feedback between T_r -derived I_{SM} with T_0 , g_a , and g_{cs} driven by T_r sensitivity to water stress variations.

In STIC, T_0 represents the effective temperature of the canopy-air space to which the stomata of all leaves in the canopy and non-stomatal elements (e.g., stem, soil/substrate) respond. F_E represents the fractional contribution of evaporation from the total available energy. Considering vegetation-soil-substrate as a single slab, STIC implicitly assumes the aerodynamic conductances from individual air-canopy and canopy-substrate components to be the “effective” aerodynamic conductance for energy and water vapor (i.e., g_a), and surface conductance from individual canopy (stomatal) and soil/substrate complexes to be the “effective” canopy-surface conductance (i.e., g_{cs}) which simultaneously regulates the exchanges of sensible and latent heat fluxes between the surface and the atmosphere.

By integrating T_r with standard SEB theory and vegetation biophysical principles, STIC formulates multiple state equations of T_0 , g_a , and g_{cs} to eliminate the need for any empirical parameterizations of these variables. The state equations are connected with T_r through I_{SM} , and the effects of T_r are subsequently propagated into their analytical solutions (Equations 1–4 below). These equations are based on the aerodynamic bulk transfer hypothesis, advection-aridity hypothesis (Brutsaert & Stricker, 1979), and evaporative fraction (F_E) theory (Mallick et al., 2016; Shuttleworth et al., 1989) with the detailed information for solving these equations provided in Mallick et al. (2016) and Section S1 of the Supporting Information S1.

$$F_E = \frac{2\alpha s}{2s + 2\gamma + \gamma(1 + I_{SM}) \frac{g_a}{g_{cs}}} \quad (1)$$

$$T_0 = T_a + \frac{(e_0 - e_a)(1 - F_E)}{\gamma F_E} \quad (2)$$

$$g_a = \frac{R_N - G}{\rho c_p \left[(T_0 - T_a) + \frac{(e_0 - e_a)}{\gamma} \right]} \quad (3)$$

$$g_{cs} = g_a \frac{(e_0 - e_a)}{(e_0^* - e_0)} \quad (4)$$

Here, α is the Priestley-Taylor coefficient (Priestley & Taylor, 1972), s is the slope of the saturation vapor pressure at T_a (hPa/°C), γ is the psychrometric constant (hPa/°C), e_0^* and e_0 are the saturation vapor pressure and ambient vapor pressure at the source-sink height (hPa), R_N and G are net radiation and ground heat flux (W/m²), e_a is the atmospheric vapor pressure (hPa) at the level of T_a measurement, ρ is the air density (kg/m³), and c_p is the specific heat of air at constant pressure (J/kg/K), respectively. The inputs needed for the computation of T_0 , conductances, and SEB fluxes in STIC are T_a , T_r , rH or e_a , and downwelling and reflected global radiation (R_G and R_p). Estimation of R_N follows the method of Bhattarai et al. (2018) and G follows Santanello and Friedl (2003) where the original method is modified by introducing I_{SM} in the G formulation (details provided in section S1 of Supporting Information S1). Given the estimates of I_{SM} , R_N , and G , the four state equations (Equations 1–4) can be solved simultaneously to derive their analytical solutions. However, the analytical expressions contain three accompanying unknowns: e_0 , e_0^* , and α . Therefore, an iterative solution is needed to determine the three unknown variables. Once the analytical solutions of g_a and g_{cs} are obtained, both variables are used to directly estimate E .

I_{SM} is a unitless quantity, which describes the relative wetness or the intensity of water stress on a surface. It controls the transition from potential to actual evaporation, which implies $I_{SM} \rightarrow 1$ on the unstressed surface and $I_{SM} \rightarrow 0$ on the stressed surface. Therefore, I_{SM} is critical for providing a constraint against which T_0 and the conductances are estimated. Since T_r is extremely sensitive to the surface water stress variations (Kustas et al., 2007), it is directly used for estimating I_{SM} in conjunction with air and dewpoint temperatures by exploiting the psychrometric theory of vapor pressure-temperature slope relationship. I_{SM} is expressed as a function of $[(T_{0D} - T_D)/(T_r - T_D)]$, where T_{0D} and T_D are the dewpoint temperature of the source/sink height and air, respectively (Bhattarai et al., 2018; Mallick

et al., 2016, 2018). Details of I_{SM} estimation are provided in section S1 of Supporting Information S1. In STIC, an initial value of α is assigned as 1.26; initial estimates of e_0^* are obtained from T_r through temperature-saturation vapor pressure relationship, and initial estimates of e_0 are obtained from I_{SM} as $e_0 = e_a + I_{SM}(e_0^* - e_a)$. Initial values of I_{SM} and T_{0D} are estimated according to Venturini et al. (2008), and this I_{SM} and R_N are used to approximate an initial estimate of G (see Section S1 in Supporting Information S1). With the initial estimates of these variables, first estimates of the conductances, T_0 , F_E , H , and E are obtained. The process is then iterated by updating e_0^* , e_0 , I_{SM} , and α (using Equations A9, A10, A11, A17, A16, and A15 in Mallick et al., 2016), with the first estimates of g_{cs} , g_a , T_0 , and E . This is followed by recalculation of G , g_{cs} , g_a , T_0 , F_E , H , and E in the subsequent iterations with the previous estimates of e_0^* , e_0 , I_{SM} , and α until the convergence of E is achieved. Stable values of E are typically obtained within ~ 10 – 15 iterations.

2.2. Datasets and Study Sites

We used in-situ and remote sensing observations for model simulation and analysis. Level 3 post-processed and gap-filled meteorological, soil moisture, and SEB flux observations from the EC flux tower network of Australia (OzFlux, <http://data.ozflux.org.au/portal/home.jsp>) (Beringer et al., 2016) and United States (AmeriFlux, <https://ameriflux.lbl.gov/>) (Baldocchi, 2020) is used. Surface Energy Balance fluxes, conductances, and T_0 were simulated for the years 2011–2018 for eight OzFlux and 2011–2020 for two AmeriFlux sites. The sites represent three broad ecological habitats namely arid, semiarid and mesic, covering a wide range of climate and ecosystem types (Table S1 in Supporting Information S1).

Daily clear-sky T_r observations from the Moderate resolution imaging spectroradiometer (MODIS) onboard Terra and Aqua at 1 km spatial resolution over the OzFlux sites were obtained from the European Space Agency, Climate Change Initiative (ESA CCI+) land surface temperature (LST) consortium (Ghent et al., 2019). Continuous time-series clear-sky MODIS Aqua T_r observations for the AmeriFlux sites were obtained through National Aeronautics and Space Administration (NASA) Application for Extracting and Exploring Analysis Ready Samples. In addition, the MODIS Terra-Aqua combined 4-day LAI (MCD15A2Hv006) product with a spatial resolution of 500 m was used for estimating the fractional vegetation cover (f_v).

2.3. Data Analysis

Since MODIS T_r was used to retrieve STIC T_0 , their relationship was analyzed considering different satellite view zenith angle (vza), R_G , soil water content (SWC), and f_v limits. Additional analysis and verification were also done by comparing in-situ T_r with a reference T_0 derived from EC (inverted T_0 , hereafter) (details in Text S2 of Supporting Information S1).

Inverted T_0 estimation requires information about R_G , R_r , T_a , T_r , and the value of g_a , g_{cs} , respectively. For the first three variables, we directly use the observations. In-situ T_r was estimated from the observations of upwelling and downwelling longwave radiation and surface emissivity using the expression from Wang et al. (2005) (details in Text S2 of Supporting Information S1). In-situ g_a was estimated from direct observations of wind speed (u) and friction velocity (u^*) according to Verma (1989) [$g_a = (u/u^{*2} + 2/ku^*)^{-1}$, $k =$ Von Karman's constant (0.4)]. In-situ g_{cs} was estimated from R_N , G , atmospheric vapor pressure deficit (D_a) observations and g_a . A detailed description of the estimation of individual variables is provided in Text S2 of Supporting Information S1.

3. Results and Discussion

T_0 estimates from STIC and inverted T_0 were significantly correlated ($r = 0.81$ – 0.96 , $p < 0.05$) (Figures 1a–1c) for the observed range of H . However, the scatterplots revealed unequal variability of the two temperatures, particularly in arid and semiarid ecosystems. The mean bias and root mean square difference (RMSD) between the two temperatures were -3.98 to 3.26°C and 2.57 – 8.47°C , with systematic RMSD of 35%–59%. The residual difference between STIC versus inverted T_0 appeared to be robustly related to tower-based g_a estimates ($r = 0.42$ – 0.86 , $p < 0.05$) (Figure S2a–S2c in Supporting Information S1). This implies that assuming a constant kB^{-1} value of 2 in the numerator of Equation S2.9 in Supporting Information S1 does not adequately capture the expected variations in flux-inverted T_0 . However, varying kB^{-1} as a function of u and radiometric to air temperature difference

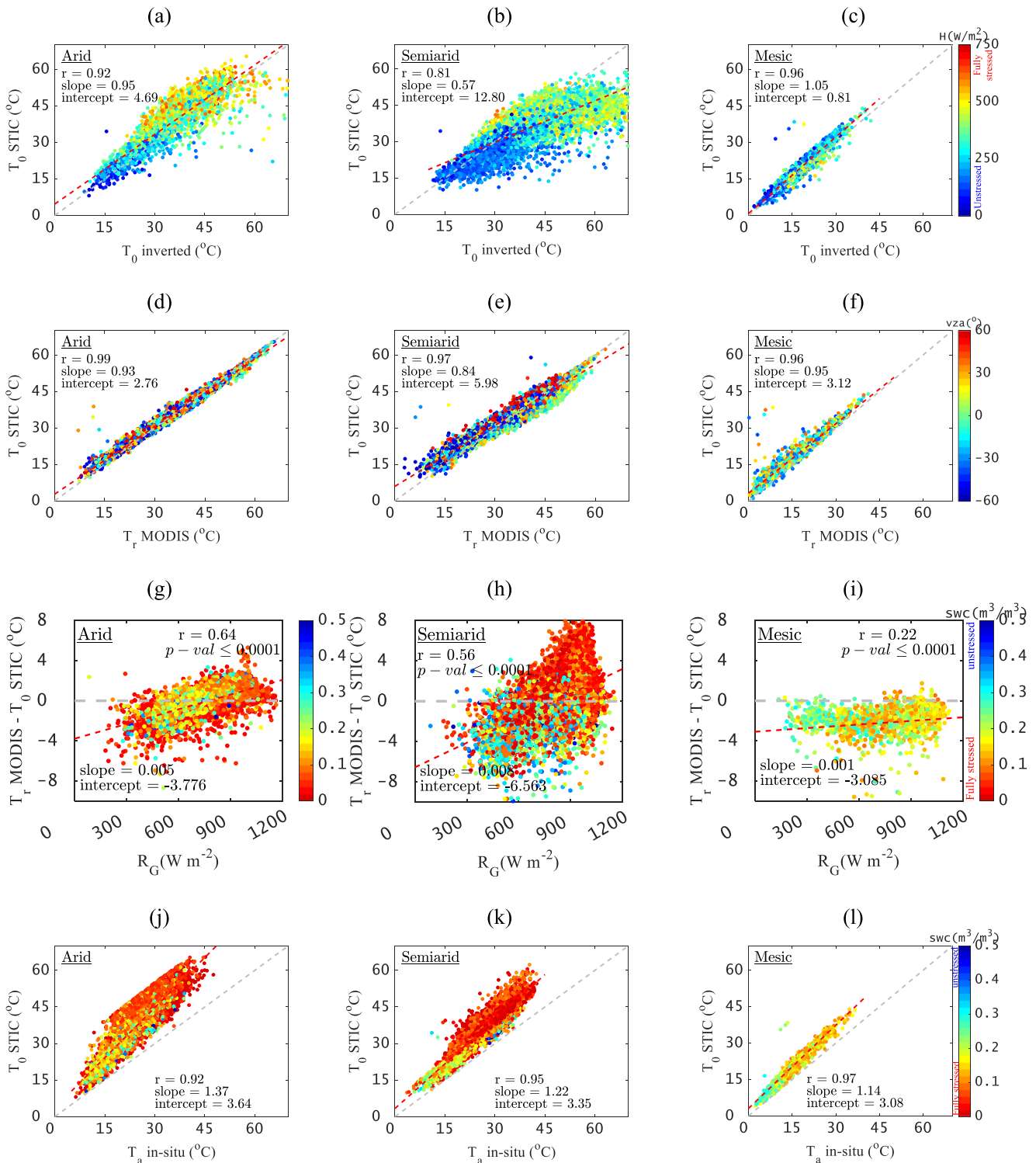


Figure 1. (a–c) Comparison between Surface Temperature Initiated Closure (STIC) T_0 versus inverted T_0 by combining data of all arid, semiarid, and mesic sites for a wide range of sensible heat flux (H) representing fully stressed to unstressed conditions. (d–f) Comparison between STIC T_0 and Moderate resolution imaging spectroradiometer (MODIS) T_r by combining data of all the arid, semiarid, and mesic sites for a wide range of view zenith angle (vza). (g–i) Scatterplot showing the relationship between T_r and T_0 differences with R_G , and (j–l) comparison between STIC T_0 versus in-situ T_a by combining data of all the arid, semiarid, and mesic sites for a wide range of soil water content (SWC) representing fully stressed to unstressed conditions. The correlation (r), slope, and intercept from the linear regression between variables on the Y and X axes (dependent and independent variable, respectively) are shown in all subplots.

(dT_r) [$kb^{-1} = 0.13udT_r$] (Kustas et al., 1989) also showed large differences between STIC and inverted T_0 in arid and semiarid ecosystems (Figure S2d–S2e in Supporting Information S1).

Interestingly, both static and dynamic kb^{-1} revealed marginal difference in the statistical metrics of STIC versus inverted T_0 in mesic ecosystems. This clearly indicates that using kb^{-1} as an empirical correction parameter for estimating T_0 introduces uncertainty over complex landscapes. Additionally, the difference in footprint size between MODIS T_r and EC tower could be partly responsible for the differences between STIC T_0 and inverted T_0 in arid and semiarid ecosystems.

A comparison between STIC T_0 and MODIS T_r revealed T_0 differed from T_r by ± 4 – 6°C in arid and semiarid ecosystems and T_0 consistently exceeded T_r in the mesic ecosystems. While their relationship ($r = 0.96$ – 0.99 , slope = 0.84 – 0.95 , intercept = 2.76 – 5.98) was independent of satellite view zenith angle (vza) variations (Figures 1d–1f), $T_r - T_0$ was significantly correlated with R_G and H for the entire range of SWC and fractional vegetation cover (f_v) in all the ecosystems ($r = 0.22$ – 0.64 , $p < 0.05$) (Figures 1g–h, Figures S3 in Supporting Information S1). In arid and semiarid ecosystems, $T_r - T_0$ increased with increasing R_G , and T_0 increasingly exceeded T_r with declining SWC at constant R_G when the magnitude of R_G was high ($>600 \text{ W m}^{-2}$). No distinct pattern between $T_r - T_0$ and R_G was found in the mesic ecosystems (Figure 1i). A comparison between the inverted T_0 and in-situ T_r also revealed very similar pattern in arid and semiarid ecosystems as found in Figures 1d–1i (Figure S4 in Supporting Information S1). Comparison between STIC T_0 versus in-situ T_a (Figure 1j–1l) revealed strong correlation between the two ($r = 0.92$ – 0.97 , $p < 0.05$) with a progressively steeper slope of regression under high aridity conditions (1.14 – 1.37).

The statistical errors (Systematic RMSD, RMSD_S; Kling Gupta Efficiency) between STIC versus inverted T_0 and the mean difference between MODIS T_r and STIC T_0 was significantly correlated with the “source-sink” height ($r = 0.37$ – 0.78 , $p < 0.05$; Figure S5 in Supporting Information S1). Nevertheless, results indicate that T_0 is retrievable with the non-parametric approach. Figure 2 (below) discusses the reasons for T_0 versus T_r inequality considering the interactions of STIC derived biophysical conductances with SEB observations for a broad range of soil and atmospheric water stress.

Depending on aridity and vegetation characteristics, evaporation response to increasing D_a varies from strongly decreasing to increasing (Massmann et al., 2019). The present study revealed two distinct patterns of $T_r - T_0$ depending on g_{cs} and F_E responses to D_a and vegetation cover. In arid and semiarid ecosystems, sparse vegetation in conjunction with high D_a , radiative heating, and water stress triggers a decline in g_{cs} (Chaves et al., 2016; Grossiord et al., 2020), F_E and humidity at the source-sink height (Figure S6 in Supporting Information S1). This leads to an elevated vapor pressure deficit at the source-sink height (D_0) ($D_0 \gg D_a$). A cascade of subsequent impacts followed an increase in H, T_a , and g_a at the cost of a decline in F_E and the g_{cs}/g_a ratio due to high $D_0 - D_a$ (Figures 2a, 2b, 2d, and 2e; Figure S7a–S7b in Supporting Information S1). The scatterplot of H versus F_E for a range of g_{cs}/g_a showed that while H increases with decreasing g_{cs}/g_a at a constant F_E , H also increases with declining F_E for a constant g_{cs}/g_a (Figures 2d and 2e). For a constant radiometric to air temperature difference (dT_r), H increases with increasing g_a ; and for a constant H, dT_r increases with decreasing g_a . However, when both g_a and H vary together, dT_r decreases with increasing H and g_a (Figure S7d–S7f in Supporting Information S1). While high g_a leads to high H at the cost of reduced F_E and g_{cs} , strong vegetation-atmospheric coupling, rising soil water stress, and high D_0 leads to an escalation of T_0 beyond T_r (Figures 2g and 2h). For sparse vegetation, when soil temperature is higher than the vegetation temperature due to a dry soil surface, T_r exceeds T_0 due to the larger impact of soil temperature on T_r (Figure S7g–S7i in Supporting Information S1) (Boulet et al., 2012; Huband & Monteith, 1986). Such behavior is a likelihood indication of biophysical homeostasis where thermoregulation and self-organization leads to optimum vegetation functioning in water-scarce environments (Kleidon, 2020; Lenton, 2003) for a given fractional canopy cover and surface to root zone water stress. The homeostasis in T_r is evidenced by a coordinated response of the canopy-surface conductance to vapor pressure deficit during high soil water stress and radiative heating of the canopy (Dong et al., 2017). However, the magnitude of T_r is well constrained by relative apportioning of evaporation and sensible heat fluxes. In mesic ecosystems with high SWC, consistently lower T_r than T_0 was due to high evaporative cooling from the transpiring vegetation (Lin et al., 2017).

Figures 2j–2l compares the evaporation (E) (as latent heat fluxes) and H derived from STIC with observations, showing good agreement with regression coefficients of 0.76 – 0.91 for H and a slightly lower correlation for E

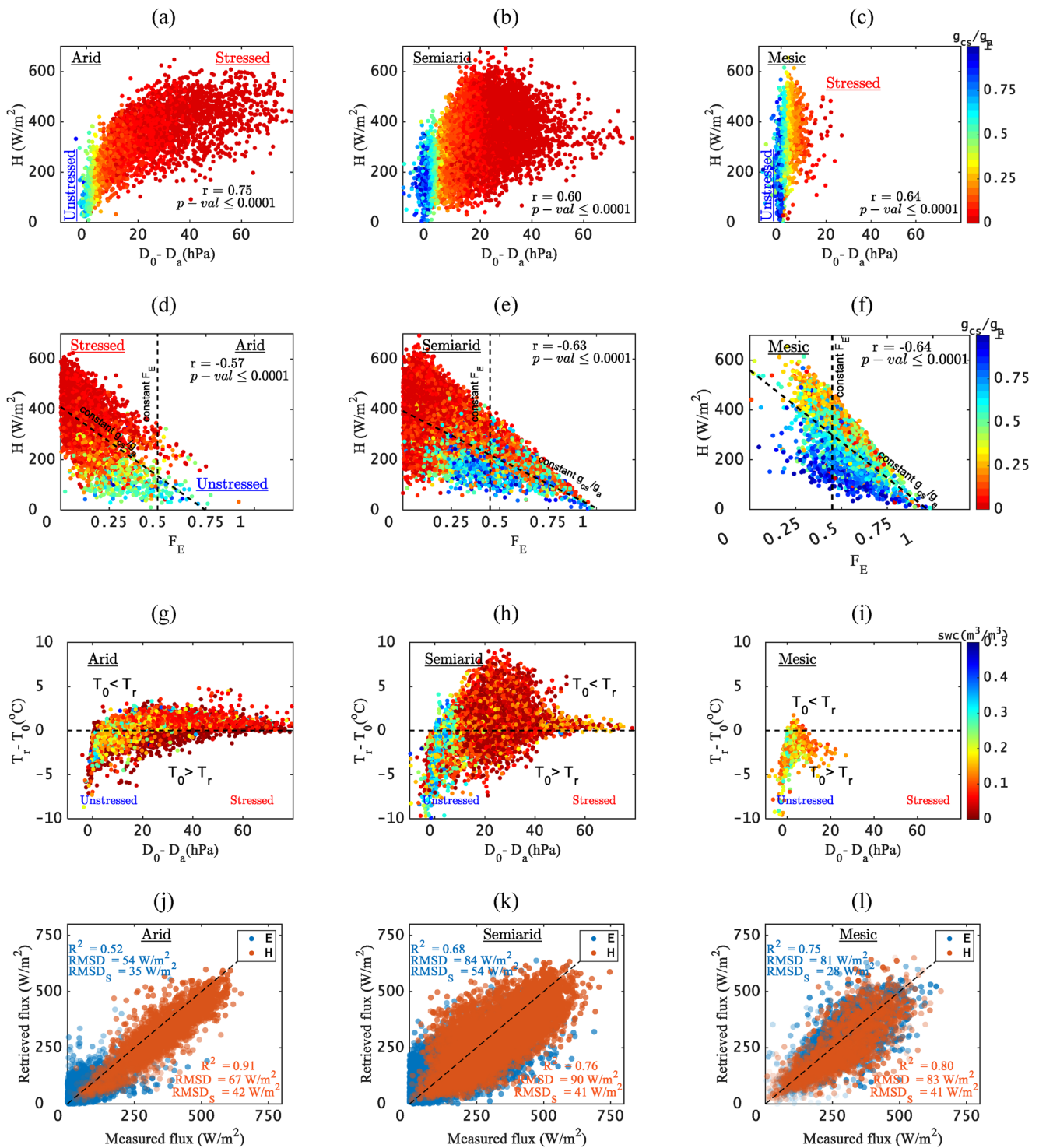


Figure 2. Scatterplots showing how the increase in source-sink height vapor pressure deficit (D_0) and its departure from D_a leads to a decline in g_{cs}/g_a ratio and evaporative fraction (F_E) at the cost of increasing the H and T_a (a–b, d–e) (also Figure S7a–S7c in Supporting Information S1). Under low to moderate fractional vegetation cover, elevated water stress and high H leads to increased T_0 and D_0 at the source-sink height (g–h), thus increasing T_0 beyond T_r (also Figure S7g–S7i in Supporting Information S1). (j–l) Retrieved versus measured E and H by combining data of all sites in an individual aridity class. root mean square difference (RMSD) and $RMSD_s$ are the root mean square difference and systematic RMSD, respectively. Formula for estimating RMSDs is given in S2 of Supporting Information S1.

(0.52–0.75). One of the major factors shaping evaporation in radiation-controlled (mesic) and water-controlled (arid and semiarid) ecosystems is the soil water availability, and STIC clearly distinguished the water stress impacts on evaporation. Water stress mainly affects g_{cs} to reduce evaporation, which is reasonably captured by STIC. Interestingly, the substantial difference in surface roughness between these ecosystems apparently had little effect on E and H retrieval through STIC.

Some limitations of our approach are worth mentioning. First, our approach does not explicitly consider the effects of atmospheric stability in the estimation of g_a . However, we anticipate such effects are embedded in the dT_r . Second, it relies on an aggregated water stress factor to derive lumped estimates of canopy-surface conductance. Retrieving a pure canopy-stomatal conductance signal needs an explicit description of soil-canopy energy balance, which tends to shed more light on this analysis. The method could also be improved by extrapolating T_a and D_a from the height of the tower above the canopy to near the canopy roughness sublayer or direct measurement of near-canopy T_a and D_a where the processes are occurring. This needs more work, which is beyond the scope of the present study. Yet, the highly explained variance of the T_0 and conductances from mid-morning and afternoon hours suggests that the non-parametric model captures the fundamental biophysical factors that shape up the SEB fluxes, thereby providing relevant insights into thermal-based evaporation modeling and land-atmosphere interactions across a large spectrum of biomes and climates.

TIR-based evaporation retrievals have been validated over the last decades using several structurally different models with diverse soil-canopy conductance parameterizations (Boulet et al., 2012; Kustas and Anderson, 2009). All the studies emphasized the pivotal role of T_0 in evaporation mapping and concluded that empirical corrections and parameterizations of the conductances to accommodate the inequality between T_0 and T_r are not appropriate to estimate evaporation over sparse canopies (Lhomme et al., 1997; Troufleau et al., 1997). These parameterizations are not stationary and vary with vegetation structure, water stress and climatic conditions, and they should therefore be used with caution before being implemented in an operational manner (Bhattarai et al., 2018; Kustas et al., 2007; Trebs et al., 2021; Verhoef et al., 1997). We advance the understanding that the inequality between T_0 and T_r is primarily regulated by water stress induced variations in canopy-surface conductance and evaporation in arid and semiarid ecosystems under varying vegetation cover, along with their subsequent influence on sensible heat flux, air temperature and aerodynamic conductance. Surface Temperature Initiated Closure reproduces the variability in T_0 , conductances, and evaporation across the seasons and over highly contrasting climate and biomes. It is somewhat remarkable that H was relatively less dynamic as compared to evaporation across different ecosystems, despite contrasting water availability and surface roughness. This indicates that surface roughness is also likely to play a significant role in shaping the interactions between the T_0 and conductances. Such interactions are likely to be reproduced in STIC, despite not explicitly incorporating any surface roughness parameterization. This suggests that from the reliable information of available energy and water stress limits, it is possible to understand the differences between T_0 and T_r while simplifying the complexities in TIR-based evaporation modeling. The non-parametric framework of STIC sets the available energy and water limits through T_r , coupled to the overlying atmospheric radiation, T_a and D_a , which is why the interactions between conductances, evaporation and T_0 are explained without the need for knowing wind speed information or applying corrections for atmospheric stability.

4. Conclusion

We conclude that STIC offers a novel perspective to directly retrieve the critical temperature component of SEB model and simultaneously estimate evaporation. This novel perspective is obtained through a simplified method for thermal remote sensing based global evaporation retrieval which does not need explicit specifications of any aerodynamic surface roughness and atmospheric stability function. Our analysis revealed that the long-debated difference between T_0 and T_r is created due to the biophysical control on evaporation under soil and atmospheric water stress and resultant homeostasis in T_r . This critical insight and validation of evaporation and sensible heat flux are highly significant to the TIR Earth observation mission and evaporation monitoring community. Statistical analysis over a large range of vegetation and climate types demonstrates the potential of STIC as a valid alternative to estimate spatio-temporal variations of evaporation. This novel approach can be utilized in thermal images from current and future remote sensing missions like Ecosystem Spaceborne Thermal Radiometer Experiment on Space Station (ECOSTRESS), Thermal infraRed Imaging Satellite for High-resolution Natural resource

Assessment (TRISHNA), and Surface Biology and Geology (SBG), and to generate insightful information for the land surface modeling community.

Data Availability Statement

The MODIS Terra and Aqua land surface temperature data are available through https://gws-access.jasmin.ac.uk/public/esacci_lst/LIST/. Level-3 eddy covariance data in netcdf format over the Ozflux sites are available from <https://data.ozflux.org.au/portal/pub/viewColDetails.jsp?collection.id=152%26collection.owner.id=101%26viewType=anonymous> (ASM), <https://data.ozflux.org.au/portal/pub/viewColDetails.jsp?collection.id=1882712%26collection.owner.id=703%26viewType=anonymous> (CPR), <https://data.ozflux.org.au/portal/pub/viewColDetails.jsp?collection.id=750%26collection.owner.id=503%26viewType=anonymous> (GWW), <https://data.ozflux.org.au/portal/pub/viewColDetails.jsp?collection.id=1883250%26collection.owner.id=768%26viewType=anonymous> (Gin), <https://data.ozflux.org.au/portal/pub/viewColDetails.jsp?collection.id=1882702%26collection.owner.id=304%26viewType=anonymous> (Dry), <https://data.ozflux.org.au/portal/pub/viewColDetails.jsp?collection.id=1882705%26collection.owner.id=304%26viewType=anonymous> (Stp), <https://data.ozflux.org.au/portal/pub/viewColDetails.jsp?collection.id=1882717%26collection.owner.id=2022264%26viewType=anonymous> (Tum), and <https://data.ozflux.org.au/portal/pub/viewColDetails.jsp?collection.id=1882713%26collection.owner.id=2021351%26viewType=anonymous> (Wom), respectively. Eddy covariance data in csv format over the Ameriflux sites are available from https://ameriflux.lbl.gov/login/?redirect_to=/data/download-data/?request=policy:CCBY4.0;site_id:US-Var and https://ameriflux.lbl.gov/login/?redirect_to=/data/download-data/?request=policy:CCBY4.0;site_id:US-Ton through Ameriflux registration. Harmonized time series datasets over the study grids and codes of the analysis are available in Zenodo (<https://doi.org/10.5281/zenodo.6720146>).

Acknowledgments

KM acknowledges the funding from ESA CCI+ Phase I New ECVS LST (ESA/Contract No. 400123553/18/I-NB), SMARTIES funding through FNR-PRIMA (INTER/PRIMA/19/13566440/SMARTIES), and Mobility Fellowship from the FNR Luxembourg (INTER/MOBILITY/2020/14521920/MONASTIC). MS acknowledges the financial support from the FNR CORE programme (CAPACITY, C19/SR/13652816). DDB acknowledges support from NASA Ecostress project and the US Department of Energy, Office of Science which supports the Ameriflux project. The OzFlux and Supersite network is supported by the National Collaborative Infrastructure Strategy through the Terrestrial Ecosystem Research Network. WW is supported by an Australian Research Council DECRA Fellowship (DE190101182). Mention of trade of names or commercial products in this publication is solely for the purpose of providing specific information and does not imply recommendation or endorsement by the U.S. Department of Agriculture. USDA is an equal opportunity provider and employer.

References

- Bai, Y., Zhang, S., Bhattarai, N., Mallick, K., Liu, Q., Tang, L., et al. (2021). On the use of machine learning based ensemble approaches to improve evapotranspiration estimates from croplands across a wide environmental gradient. *Agricultural and Forest Meteorology*, 298, 108308. <https://doi.org/10.1016/j.agrformet.2020.108308>
- Baldocchi, D. D. (2020). How eddy covariance flux measurements have contributed to our understanding of Global Change Biology. *Global Change Biology*, 26(1), 242–260. <https://doi.org/10.1111/gcb.14807>
- Beringer, J., Hutley, L. B., McHugh, I., Arndt, S. K., Campbell, D., Cleugh, H. A., et al. (2016). An introduction to the Australian and New Zealand flux tower network—OzFlux. *Biogeosciences*, 13(21), 5895–5916. <https://doi.org/10.5194/bg-13-5895-2016>
- Bhattarai, N., Mallick, K., Brunsell, N. A., Sun, G., & Jain, M. (2018). Regional evapotranspiration from an image-based implementation of the Surface Temperature Initiated Closure (STIC1. 2) model and its validation across an aridity gradient in the conterminous US. *Hydrology and Earth System Sciences*, 22(4), 2311–2341. <https://doi.org/10.5194/hess-22-2311-2018>
- Bhattarai, N., Mallick, K., Stuart, J., Vishwakarma, B. D., Niraula, R., Sen, S., & Jain, M. (2019). An automated multi-model evapotranspiration mapping framework using remotely sensed and reanalysis data. *Remote Sensing of Environment*, 229, 69–92. <https://doi.org/10.1016/j.rse.2019.04.026>
- Boulet, G., Olioso, A., Ceschia, E., Marloie, O., Coudert, B., Rivalland, V., et al. (2012). An empirical expression to relate aerodynamic and surface temperatures for use within single-source energy balance models. *Agricultural and Forest Meteorology*, 161, 148–155. <https://doi.org/10.1016/j.agrformet.2012.03.008>
- Brutsaert, W., & Stricker, H. (1979). An advection-aridity approach to estimate actual regional evapotranspiration. *Water Resources Research*, 15(2), 443–450. <https://doi.org/10.1029/wr015i002p00443>
- Chaves, M. M., Costa, J. M., Zarrouk, O., Pinheiro, C., Lopes, C. M., & Pereira, J. S. (2016). Controlling stomatal aperture in semi-arid regions—The dilemma of saving water or being cool? *Plant Science*, 251, 54–64. <https://doi.org/10.1016/j.plantsci.2016.06.015>
- Chebouni, A., Nouvellon, Y., Lhomme, J. P., Watts, C., Boulet, G., Kerr, Y. H., et al. (2001). Estimation of surface sensible heat flux using dual angle observations of radiative surface temperature. *Agricultural and Forest Meteorology*, 108(1), 55–65. [https://doi.org/10.1016/S0168-1923\(01\)00221-0](https://doi.org/10.1016/S0168-1923(01)00221-0)
- Chebouni, A., Seen, D. L., Njoku, E. G., & Monteny, B. M. (1996). Examination of the difference between radiative and aerodynamic surface temperatures over sparsely vegetated surfaces. *Remote Sensing of Environment*, 58(2), 177–186. [https://doi.org/10.1016/S0034-4257\(96\)00037-5](https://doi.org/10.1016/S0034-4257(96)00037-5)
- Dong, N., Prentice, I. C., Harrison, S. P., Song, Q. H., Zhang, Y. P., & Sykes, M. (2017). Biophysical homeostasis of leaf temperature: A neglected process for vegetation and land-surface modelling. *Global Ecology and Biogeography*, 26(9), 998–1007. <https://doi.org/10.1111/geb.12614>
- Garratt, J. R., & Hicks, B. B. (1973). Momentum, heat and water vapour transfer to and from natural and artificial surfaces. *Quarterly Journal of the Royal Meteorological Society*, 99(422), 680–687. <https://doi.org/10.1002/qj.49709942209>
- Ghent, D., Veal, K., Trent, T., Dodd, E., Sembhi, H., & Remedios, J. (2019). A new approach to defining uncertainties for MODIS land surface temperature. *Remote Sensing*, 11(9), 1021. <https://doi.org/10.3390/rs11091021>
- Grossiord, C., Buckley, T. N., Cernusak, L. A., Novick, K. A., Poulter, B., Siegwolf, R. T. W., et al. (2020). Plant responses to rising vapor pressure deficit. *New Phytologist*, 226(6), 1550–1566. <https://doi.org/10.1111/nph.16485>
- Huband, N. D. S., & Monteith, J. L. (1986). Radiative surface temperature and energy balance of a wheat canopy. *Boundary-Layer Meteorology*, 36(1–2), 1–17. <https://doi.org/10.1007/bf00117455>

- Kleidon, A. (2020). Understanding the Earth as a whole system: From the Gaia hypothesis to thermodynamic optimality and human societies. <https://doi.org/10.48550/arXiv.2005.09216>
- Kustas, W., & Anderson, M. (2009). Advances in thermal infrared remote sensing for land surface modeling. *Agricultural and Forest Meteorology*, *149*(12), 2071–2081. <https://doi.org/10.1016/j.agrformet.2009.05.016>
- Kustas, W. P., Anderson, M. C., Norman, J. M., & Li, F. (2007). Utility of radiometric–aerodynamic temperature relations for heat flux estimation. *Boundary-Layer Meteorology*, *122*(1), 167–187. <https://doi.org/10.1007/s10546-006-9093-1>
- Kustas, W. P., Choudhury, B. J., Moran, M. S., Reginato, R. J., Jackson, R. D., Gay, L. W., & Weaver, H. L. (1989). Determination of sensible heat flux over sparse canopy using thermal infrared data. *Agricultural and Forest Meteorology*, *44*(3–4), 197–216. [https://doi.org/10.1016/0168-1923\(89\)90017-8](https://doi.org/10.1016/0168-1923(89)90017-8)
- Lenton, T. (2003). Gaia hypothesis. In *Encyclopedia of atmospheric sciences* (pp. 815–820).
- Lhomme, J. P., Troufleau, D., Monteny, B., Chehbouni, A., & Bauduin, S. (1997). Sensible heat flux and radiometric surface temperature over sparse Sahelian vegetation II. A model for the kb-1 parameter. *Journal of Hydrology*, *188*, 839–854. [https://doi.org/10.1016/s0022-1694\(96\)03173-3](https://doi.org/10.1016/s0022-1694(96)03173-3)
- Li, Y., Kustas, W. P., Huang, C., Nieto, H., Haghighi, E., Anderson, M. C., et al. (2019). Evaluating soil resistance formulations in thermal-based two-source energy balance (TSEB) model: Implications for heterogeneous semiarid and arid regions. *Water Resources Research*, *55*(2), 1059–1078. <https://doi.org/10.1029/2018wr022981>
- Lin, H., Chen, Y., Song, Q., Fu, P., Cleverly, J., Magliulo, V., et al. (2017). Quantifying deforestation and forest degradation with thermal response. *Science of the Total Environment*, *607*, 1286–1292. <https://doi.org/10.1016/j.scitotenv.2017.07.062>
- Mallick, K., Jarvis, A. J., Boegh, E., Fisher, J. B., Drewry, D. T., Tu, K. P., et al. (2014). A Surface Temperature Initiated Closure (STIC) for surface energy balance fluxes. *Remote Sensing of Environment*, *141*, 243–261. <https://doi.org/10.1016/j.rse.2013.10.022>
- Mallick, K., Toivonen, E., Trebs, I., Boegh, E., Cleverly, J., Eamus, D., et al. (2018). Bridging thermal infrared sensing and physically-based evapotranspiration modeling: From theoretical implementation to validation across an aridity gradient in Australian ecosystems. *Water Resources Research*, *54*(5), 3409–3435. <https://doi.org/10.1029/2017wr021357>
- Mallick, K., Trebs, I., Boegh, E., Giustarini, L., Schlerf, M., Drewry, D. T., et al. (2016). Canopy-scale biophysical controls of transpiration and evaporation in the Amazon Basin. *Hydrology and Earth System Sciences*, *20*(10), 4237–4264. <https://doi.org/10.5194/hess-20-4237-2016>
- Massmann, A., Gentine, P., & Lin, C. (2019). When does vapor pressure deficit drive or reduce evapotranspiration? *Journal of Advances in Modeling Earth Systems*, *11*(10), 3305–3320. <https://doi.org/10.1029/2019ms001790>
- Priestley, C. H. B., & Taylor, R. J. (1972). On the assessment of surface heat flux and evaporation using large-scale parameters. *Monthly Weather Review*, *100*(2), 81–92. [https://doi.org/10.1175/1520-0493\(1972\)100<0081:otaosh>2.3.co;2](https://doi.org/10.1175/1520-0493(1972)100<0081:otaosh>2.3.co;2)
- Santanello, J. A., Jr., & Friedl, M. A. (2003). Diurnal covariation in soil heat flux and net radiation. *Journal of Applied Meteorology*, *42*(6), 851–862. [https://doi.org/10.1175/1520-0450\(2003\)042<0851:dcisfh>2.0.co;2](https://doi.org/10.1175/1520-0450(2003)042<0851:dcisfh>2.0.co;2)
- Shuttleworth, W. J., Gurney, R. J., Hsu, A. Y., & Ormsby, J. P. (1989). FIFE: The variation in energy partition at surface flux sites. *IAHS Publication*, *186*, 523–534.
- Trebs, I., Mallick, K., Bhattarai, N., Sulis, M., Cleverly, J., Woodgate, W., et al. (2021). The role of aerodynamic resistance in thermal remote sensing-based evapotranspiration models. *Remote Sensing of Environment*, *264*, 112602. <https://doi.org/10.1016/j.rse.2021.112602>
- Troufleau, D., Lhomme, J.-P., Monteny, B., & Vidal, A. (1997). Sensible heat flux and radiometric surface temperature over sparse Sahelian vegetation I. An experimental analysis of the kb-1 parameter. *Journal of Hydrology*, *188*, 815–838. [https://doi.org/10.1016/s0022-1694\(96\)03172-1](https://doi.org/10.1016/s0022-1694(96)03172-1)
- Venturini, V., Islam, S., & Rodriguez, L. (2008). Estimation of evaporative fraction and evapotranspiration from MODIS products using a complementary based model. *Remote Sensing of Environment*, *112*(1), 132–141. <https://doi.org/10.1016/j.rse.2007.04.014>
- Verhoef, A., De Bruin, H. A. R., & Van Den Hurk, B. (1997). Some practical notes on the parameter kb-1 for sparse vegetation. *Journal of Applied Meteorology*, *36*(5), 560–572. [https://doi.org/10.1175/1520-0450\(1997\)036<0560:spnotp>2.0.co;2](https://doi.org/10.1175/1520-0450(1997)036<0560:spnotp>2.0.co;2)
- Verma, S. B. (1989). Aerodynamic resistances to transfers of heat, mass and momentum. In *Proceedings of a workshop held at Vancouver* (pp. 13–20). IAHS Publ.
- Wang, K., Wan, Z., Wang, P., Sparrow, M., Liu, J., Zhou, X., & Haginoya, S. (2005). Estimation of surface long wave radiation and broadband emissivity using moderate resolution imaging spectroradiometer (MODIS) land surface temperature/emissivity products. *Journal of Geophysical Research*, *110*(D11), D11109. <https://doi.org/10.1029/2004jd005566>
- Young, A. M., Friedl, M. A., Seyednasrollah, B., Beamesderfer, E., Carrillo, C. M., Li, X., et al. (2021). Seasonality in aerodynamic resistance across a range of North American ecosystems. *Agricultural and Forest Meteorology*, *310*, 108613. <https://doi.org/10.1016/j.agrformet.2021.108613>

References From the Supporting Information

- Choudhury, B. J., & Monteith, J. L. (1986). Implications of stomatal response to saturation deficit for the heat balance of vegetation. *Agricultural and Forest Meteorology*, *36*(3), 215–225. [https://doi.org/10.1016/0168-1923\(86\)90036-5](https://doi.org/10.1016/0168-1923(86)90036-5)
- Mallick, K., Boegh, E., Trebs, I., Alfieri, J. G., Kustas, W. P., Prueger, J. H., et al. (2015). Reintroducing radiometric surface temperature into the Penman-Monteith formulation. *Water Resources Research*, *51*(8), 6214–6243. <https://doi.org/10.1002/2014wr016106>
- Monteith, J. L. (1965). Evaporation and environment. In *Symposia of the society for experimental biology* (Vol. 19, pp. 205–234). Cambridge University Press (CUP).
- Penman, H. L. (1948). Natural evaporation from open water, bare soil and grass. *Proceedings of the Royal Society of London. Series A. Mathematical and Physical Sciences*, *193*, 120–145.
- Rogelis, M. C., Werner, M., Obregón, N., & Wright, N. (2016). Hydrological model assessment for flood early warning in a tropical high mountain basin. In *Hydrology and Earth system sciences discussions* (pp. 1–36).
- Schymanski, S. J., & Or, D. (2017). Leaf-scale experiments reveal an important omission in the Penman–Monteith equation. *Hydrology and Earth System Sciences*, *21*(2), 685–706. <https://doi.org/10.5194/hess-21-685-2017>